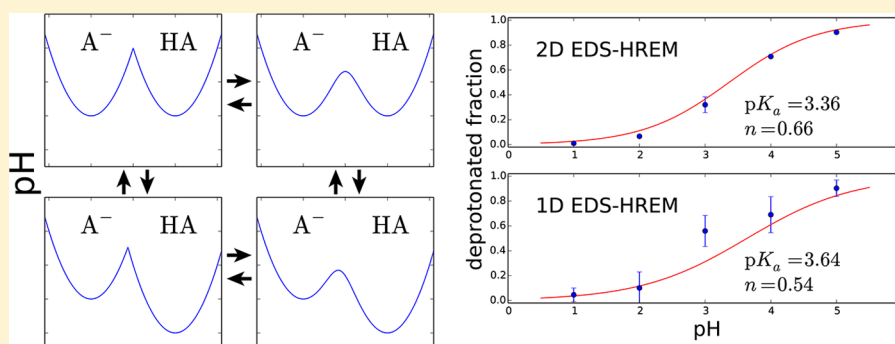


Enhancing Constant-pH Simulation in Explicit Solvent with a Two-Dimensional Replica Exchange Method

Juyong Lee,^{*,†} Benjamin T. Miller,[†] Ana Damjanović,^{†,‡} and Bernard R. Brooks[†][†]Laboratory of Computational Biology, National Heart, Lung, and Blood Institute, National Institutes of Health, Bethesda, Maryland 20892, United States[‡]Department of Biophysics, Johns Hopkins University, Baltimore, Maryland 21218, United States

S Supporting Information



ABSTRACT: We present a new method for enhanced sampling for constant-pH simulations in explicit water based on a two-dimensional (2D) replica exchange scheme. The new method is a significant extension of our previously developed constant-pH simulation method, which is based on enveloping distribution sampling (EDS) coupled with a one-dimensional (1D) Hamiltonian exchange method (HREM). EDS constructs a hybrid Hamiltonian from multiple discrete end state Hamiltonians that, in this case, represent different protonation states of the system. The ruggedness and heights of the hybrid Hamiltonian's energy barriers can be tuned by the smoothness parameter. Within the context of the 1D EDS-HREM method, exchanges are performed between replicas with different smoothness parameters, allowing frequent protonation-state transitions and sampling of conformations that are favored by the end-state Hamiltonians. In this work, the 1D method is extended to 2D with an additional dimension, external pH. Within the context of the 2D method (2D EDS-HREM), exchanges are performed on a lattice of Hamiltonians with different pH conditions and smoothness parameters. We demonstrate that both the 1D and 2D methods exactly reproduce the thermodynamic properties of the semigrand canonical (SGC) ensemble of a system at a given pH. We have tested our new 2D method on aspartic acid, glutamic acid, lysine, a four residue peptide (sequence KAAE), and snake cardiotoxin. In all cases, the 2D method converges faster and without loss of precision; the only limitation is a loss of flexibility in how CPU time is employed. The results for snake cardiotoxin demonstrate that the 2D method enhances protonation-state transitions, samples a wider conformational space with the same amount of computational resources, and converges significantly faster overall than the original 1D method.

1. INTRODUCTION

Solution pH is one of the most important environmental factors that affects the structure and dynamics of proteins.^{1,2} Almost all biologically relevant properties of proteins are affected by pH: stability, folding and assembly, interactions with ligands and other biological molecules, solubility, aggregation properties, and enzymatic activity. A change in pH may induce a change in the protonation state of ionizable groups, which in turn can cause structural changes in proteins.³ Structural changes triggered by protonation/deprotonation can be exploited for function, such as in the case of ATP synthase,^{4–6} bacteriorhodopsin,⁷ cytochrome *c* oxidase,⁸ or the photoactive yellow protein.⁹

The pK_a values of ionizable amino acid residues in proteins can be shifted several pH units from the pK_a values that these

groups exhibit in a purely aqueous environment.^{10,11} A widely used methodology for calculating pK_a values is based on the solution of the Poisson–Boltzmann (PB) equation. However, PB-based models rely on a single value of the dielectric constant of the protein and do not properly treat structural changes; most PB-based methods use only a single conformation or allow for perturbation of side chains only.^{12–15} Conventional molecular dynamics (MD) simulations, on the other hand, can treat protein structural reorganization but depend on a fixed charge model where the charges are determined beforehand. Because protonation states can be affected by protein conformation, and protein conformation

Received: December 5, 2014

Published: May 7, 2015

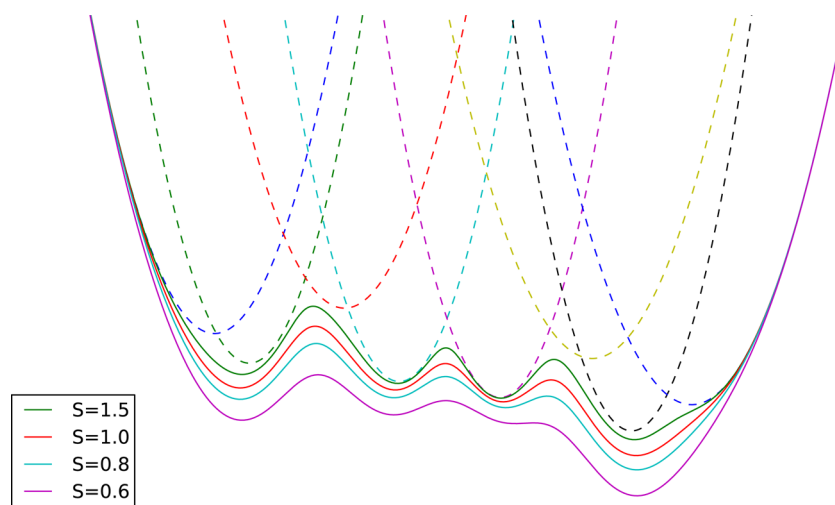


Figure 1. Schematic representation of EDS potential surfaces enveloping eight different states with different smoothness parameters. Dotted lines represent the original states, and solid lines represent the EDS potentials.

can be affected by protonation states, it becomes obvious that changes in both should be allowed in a single simulation for accurate description of the protonation/conformation equilibria. To achieve this, various constant-pH simulation methods have been devised.^{16–31} Within the context of such methods, protonation states of ionizable residues can be changed during the course of the molecular dynamics run.

Constant-pH MD simulation methods can be classified into two types: (1) discrete protonation state models and (2) continuous protonation state models. In discrete protonation state models,^{16–18,20,29} protonation states are modeled more realistically; i.e., titratable groups can be either protonated (protonation state 1) or deprotonated (protonation state 0). In continuous protonation state models^{19,21,26,27} protonation states can take any value between fully protonated or fully deprotonated. Simulations with discrete protonation states are usually performed through a combination of MD for conformational search and Monte Carlo (MC) moves to change protonation states. Unfortunately, in such simulations, it is virtually impossible to achieve change in protonation states if explicit water molecules are employed. This is because water molecules reorient to favor the current protonation state. Traditionally, simulations with discrete protonation states have been performed either with less realistic implicit solvents^{18–20} or through a combined use of explicit solvent to perform MD simulations and implicit solvent to perform MC moves.^{16,22,25,30} While it is possible to perform constant-pH simulations in explicit solvent with methods based on continuous protonation states,^{26,27} such methods are less precise since the system has to spend time in unphysical protonation states.^{19,21,23,32}

Recently, we have developed a *discrete-state* constant-pH simulation method that can be used with explicit solvent,³³ EDS-HREM, which is based on the combination of enveloping distribution sampling (EDS)^{34,35} with the Hamiltonian replica exchange method (HREM).³⁶ The EDS method generates a hybrid Hamiltonian from the Hamiltonians of multiple end states, which allows the sampling of multiple conditions in a single molecular dynamics simulation. In the case of constant-pH simulations, the end states correspond to the different protonation states that are to be sampled. A smoothing parameter governs the height and steepness of the energy

barrier between end states; a smoothed hybrid Hamiltonian can thus enhance end-state sampling.

Hamiltonian replica exchange may be used to swap conformations between more and less smoothed hybrid Hamiltonians. The primary advantage of this approach is that a very smooth hybrid Hamiltonian can be used for rapid conformational search while a completely unsmoothed Hamiltonian, which exactly follows the minimum energy end-state Hamiltonian, is sampled. This allows the simulation to converge to an exact semigrand canonical (SGC) ensemble. However, this benefit comes at the cost of requiring multiple replicas of the system to be simulated simultaneously.

An additional limitation of EDS-HREM is that sampling is only enhanced by increasing the smoothness of some replicas. In contrast, more traditional pH replica exchange methods^{24,25,28,30} allow for the simulation of multiple pH values simultaneously, which allows the propagation of structures simulated under different physical conditions. These methods enhance convergence of pK_a results by exploring a wider set of conformations. The EDS-based methodology only improves sampling along degrees of freedom that differ between end-state Hamiltonians. For example, sampling of a high side chain rotation barrier that is identically present in all end states will not be improved by EDS-HREM.

In order to overcome this obstacle and provide better sampling of the accessible titration states, we have devised a two-dimensional (2D) Hamiltonian exchange scheme. With this method, replicas are exchanged both between different EDS potentials and between different pH conditions. If the number of smoothed replicas is identical to that of 1D EDS-HREM at each pH, this procedure is no more expensive in terms of total CPU time than performing separate EDS Hamiltonian replica exchange simulations at each pH value. The only added restriction is that all pH values must be simulated simultaneously so that exchanges may occur. Similar two-dimensional replica exchange ideas^{37–40} have been applied to address other problems including protein–protein interaction,^{41,42} refinement of loop structure,⁴³ sampling RNA tetranucleotide conformations,⁴⁴ and protein–ligand binding.⁴⁵

We assessed the performance of our new scheme with titratable amino acid monomers, a short peptide with four possible protonation states, and snake cardiotoxin (1CVO).^{46,47}

The results of these simulations show that two-dimensional exchange substantially improves the convergence of constant-pH simulations. We also show that the improved convergence of the new scheme is due to an increased number of protonation-state transitions especially at pH values that differ from pK_a values, and broader conformational sampling. Our new constant-pH simulation method is a state-based method and yields an accurate ensemble of a titratable system, which makes it suitable for free energy calculations.

2. METHODS

2.1. Constant-pH Simulation with Enveloping Distribution Sampling and Hamiltonian Replica Exchange.

When used in constant-pH simulation,³³ an EDS Hamiltonian connecting a total of N different protonation states, representing the configuration of one or more individual protonation sites, is defined as

$$E_{\text{EDS}}(\mathbf{x}, s, \text{pH}) = -(\beta s)^{-1} \ln \left(\sum_{i=1}^N \exp[-\beta s(E_i(\mathbf{x}) - E_i^{\text{offset}}(\text{pH}))] \right) \quad (1)$$

where $E_i(\mathbf{x})$ is the potential energy of state i at coordinates \mathbf{x} , $\beta = (k_B T)^{-1}$, s is the smoothness parameter, and $E_i^{\text{offset}}(\text{pH})$ value is the pH-dependent energy offset value for state i . A small s value leads to a smoother energy landscape and lower energy barriers between states, which facilitates state transitions. Examples of EDS potentials enveloping $N = 8$ states, which correspond to a system with 3 uncoupled protonation sites, with different s values are illustrated in Figure 1.

It should be noted that, when there are N titratable groups, considering all 2^N possible protonation states is unnecessary. Many of the states are high in energy under certain circumstances and can be safely omitted in a free energy cycle. For example, when looking at the two aspartic groups in the HIV protease active site, we need only consider deprotonated and singly protonated states, thus reducing the complexity from 16 possible states to only 5.⁴⁸ Also, empirical pK_a prediction methods^{49,50} can be used to select titratable groups whose protonation states may change at a given pH condition.

2.1.1. Baseline Hamiltonian Following the Minimum of End-State Hamiltonians. To obtain the accurate conformational ensembles of end states, we devised a baseline Hamiltonian where the smoothness parameter $1/s$ is set to 0. Assume that state i with Hamiltonian E'_i has the lowest energy at \mathbf{x} among $\{E'_1, \dots, E'_N\}$,

$$E^0(\mathbf{x}; 1/s=0) = \lim_{1/s \rightarrow 0} -s\beta^{-1} \ln \left\{ \sum_{j=1}^N \exp[-s\beta E'_j(\mathbf{x})] \right\} \quad (2)$$

$$= E'_i(\mathbf{x}) - \lim_{1/s \rightarrow 0} [s\beta^{-1} \quad (3)$$

$$\times \ln \{ 1 + \sum_{j \neq i} \exp[-s\beta(E'_j(\mathbf{x}) - E'_i(\mathbf{x}))] \}$$

$$= \min(E'_1(\mathbf{x}), \dots, E'_N(\mathbf{x})) = E'_i(\mathbf{x}) \quad (4)$$

All exponential terms in eq 3 vanish as $1/s \rightarrow 0$ because $-s\beta(E'_j - E'_i)$ becomes a large negative number. Thus, performing MD simulations with E^0 yields conformations that follow the minimum energy surface of the initial N end-state Hamiltonians.

The advantage of this baseline Hamiltonian is that it maximizes the overlap with the original end-state Hamiltonians, which makes the resulting ensemble easy to use with other postprocessing methods. For example, a recently suggested non-Boltzmann Bennett acceptance ratio method enables one to calculate free energy differences based on quantum mechanics (QM) or quantum mechanics/molecular mechanics (QM/MM) energies via a reweighting scheme.⁵¹ This approach requires a certain extent of overlap between Hamiltonians.

However, because the baseline Hamiltonian strictly follows the end-state Hamiltonians, it has large energy barriers, which retard frequent protonation-state transitions. To overcome this sampling problem, the baseline Hamiltonian is combined with smoothed hybrid Hamiltonians via Hamiltonian replica exchange. The smoothed hybrid Hamiltonians are introduced to facilitate frequent state transitions, and, with a proper exchange criterion, the Hamiltonian exchange scheme guarantees that the canonical ensembles of various Hamiltonians are obtained.

2.1.2. Equivalence between a Baseline EDS Ensemble and the Semigrand Canonical Ensemble. If we assume a simple system with a single titratable site in equilibrium at constant pH, volume, and temperature, and the coordinates and momentum are denoted as \mathbf{x} and \mathbf{p} , respectively, the partition function of the semigrand canonical (SGC) ensemble of the system^{16,52,53} is

$$\Xi = \iint d\mathbf{x} d\mathbf{p} \exp(-\beta H_d(\mathbf{x}, \mathbf{p})) + \exp(-\beta H_p(\mathbf{x}, \mathbf{p})) \quad (5)$$

$$= \iint d\mathbf{x} d\mathbf{p} \exp(-\beta[H_d^{\text{MM}}(\mathbf{x}, \mathbf{p}) + H_d^{\text{QM}}]) + \exp(-\beta[H_p^{\text{MM}}(\mathbf{x}, \mathbf{p}) + H_p^{\text{QM}} - \mu]) \quad (6)$$

where H_d and H_p are the Hamiltonians of the deprotonated and protonated states, H^{MM} and H^{QM} correspond to the MM and QM Hamiltonians of the system, and μ is the chemical potential of a proton. H^{QM} includes hydrogen bond formation and breaking energies and is assumed to be independent from \mathbf{x} and \mathbf{p} . Based on the classical mechanics model, $H^{\text{MM}}(\mathbf{x}, \mathbf{p}) = E^{\text{MM}}(\mathbf{x}) + K^{\text{MM}}(\mathbf{p})$, the integral of the kinetic term, $\sum_{i=1}^{N_{\text{atom}}} \int \exp(-\beta p_i^2/m_i) d\mathbf{p}$, can be easily obtained analytically and becomes constant. From the SGC partition function Ξ , the probability of sampling the deprotonated state of a conformation \mathbf{x} is

$$P_{\text{SGC}}(d, \mathbf{x}) = \Xi^{-1} \int d\mathbf{p} \exp(-\beta[H_d^{\text{MM}}(\mathbf{x}, \mathbf{p}) + H_d^{\text{QM}}]) \quad (7)$$

$$= \frac{\exp(-\beta E_d^{\text{MM}}(\mathbf{x}))}{\int \exp(-\beta E_d^{\text{MM}}(\mathbf{x})) + \exp(-\beta[E_p^{\text{MM}}(\mathbf{x}) + H_p^{\text{QM}} - H_d^{\text{QM}} - \mu]) d\mathbf{x}} \quad (8)$$

$$= \frac{\exp(-\beta E_d^{\text{MM}}(\mathbf{x}))}{\int \exp(-\beta E_d^{\text{MM}}(\mathbf{x})) + \exp(-\beta[E_p^{\text{MM}}(\mathbf{x}) - E^{\text{offset}}]) d\mathbf{x}} \quad (9)$$

where $E^{\text{offset}} = -H_p^{\text{QM}} + H_d^{\text{QM}} + \mu$. Similarly, the probability of sampling the protonated state of a conformation \mathbf{x} is

$$P_{\text{SGC}}(p, \mathbf{x}) = \Xi^{-1} \int d\mathbf{p} \exp(-\beta[H_p^{\text{MM}}(\mathbf{x}, \mathbf{p}) + H_p^{\text{QM}} - \mu]) \quad (10)$$

$$= \frac{\exp(-\beta[E_p^{\text{MM}}(\mathbf{x}) - E^{\text{offset}}])}{\int \exp(-\beta E_d^{\text{MM}}(\mathbf{x})) + \exp(-\beta[E_p^{\text{MM}}(\mathbf{x}) - E^{\text{offset}}]) d\mathbf{x}} \quad (11)$$

If a conformation \mathbf{x} is considered fixed, the probability of being in the deprotonated and the protonated state can be expressed as¹⁶

$$P(d\mathbf{x}) = \frac{\int d\mathbf{p} e^{-\beta H_d(\mathbf{x}, \mathbf{p})}}{\int d\mathbf{p} (e^{-\beta H_d(\mathbf{x}, \mathbf{p})} + e^{-\beta H_p(\mathbf{x}, \mathbf{p})})} \quad (12)$$

$$= \frac{1}{1 + e^{-\beta([E_p^{MM}(\mathbf{x}) - E^{\text{offset}}] - E_d^{MM}(\mathbf{x}))}} \quad (13)$$

and

$$P(p|\mathbf{x}) = \frac{\int d\mathbf{p} e^{-\beta H_p(\mathbf{x}, \mathbf{p})}}{\int d\mathbf{p} (e^{-\beta H_d(\mathbf{x}, \mathbf{p})} + e^{-\beta H_p(\mathbf{x}, \mathbf{p})})} \quad (14)$$

$$= \frac{e^{-\beta([E_p^{MM}(\mathbf{x}) - E^{\text{offset}}] - E_d^{MM}(\mathbf{x}))}}{1 + e^{-\beta([E_p^{MM}(\mathbf{x}) - E^{\text{offset}}] - E_d^{MM}(\mathbf{x}))}} \quad (15)$$

These results can be generalized to systems with multiple titratable residues. We assume that a system has K titratable residues and its protonation state is denoted as $\mathbf{n} = (n_1, n_2, n_3, \dots, n_K)$ where $n_i = 0$ if the i th residue is protonated, otherwise $n_i = 1$. The probability of a conformation \mathbf{x} being in a protonation state \mathbf{n} can be written as

$$P(\mathbf{x}, \mathbf{n}) = \frac{e^{-\beta[E(\mathbf{x}, \mathbf{n}) - E^{\text{offset}}(\mathbf{n})]}}{\sum_{\mathbf{n}} e^{-\beta[E(\mathbf{x}, \mathbf{n}) - E^{\text{offset}}(\mathbf{n})]}} \quad (16)$$

where $E(\mathbf{x}, \mathbf{n})$ is the potential energy of a protonation state \mathbf{n} at a conformation \mathbf{x} and $E^{\text{offset}}(\mathbf{n})$ is the offset energy of the protonation state \mathbf{n} .

Based on these results, the SGC ensemble average of an observable A is

$$\begin{aligned} \langle A \rangle_{\text{SGC}} &= \int A(\mathbf{x}) P_{\text{SGC}}(d, \mathbf{x}) + A(\mathbf{x}) P_{\text{SGC}}(p, \mathbf{x}) d\mathbf{x} \\ &= \frac{\int A(\mathbf{x}) (\exp(-\beta E_d^{MM}(\mathbf{x})) + \exp(-\beta[E_p^{MM}(\mathbf{x}) - E^{\text{offset}}])) d\mathbf{x}}{\int \exp(-\beta E_d^{MM}(\mathbf{x})) + \exp(-\beta[E_p^{MM}(\mathbf{x}) - E^{\text{offset}}]) d\mathbf{x}} \end{aligned} \quad (17)$$

To demonstrate the equivalence of our method to a SGC constant-pH simulation, we will show that the thermodynamic average of an observable A obtained by our method, $\langle A \rangle_{\text{EDS}}$, is identical to $\langle A \rangle_{\text{SGC}}$.

An EDS potential with $1/s = 1$ is

$$\begin{aligned} H_{\text{EDS}}(1/s=1) \\ = -\beta^{-1} \ln(\exp(-\beta H_d(\mathbf{x}, \mathbf{p})) + \exp(-\beta[H_p(\mathbf{x}, \mathbf{p}) - E^{\text{offset}}])) \end{aligned} \quad (18)$$

and its partition function becomes

$$\begin{aligned} Z_{\text{EDS}}(1/s=1) \\ = \iint d\mathbf{x} d\mathbf{p} \exp(-\beta H_d(\mathbf{x}, \mathbf{p})) + \exp(-\beta[H_p(\mathbf{x}, \mathbf{p}) - E^{\text{offset}}]) \end{aligned} \quad (19)$$

which can be reduced to the partition function of the SGC ensemble (eq 6) assuming that the offset energy E^{offset} in eq 20 corresponds to the quantum mechanical contributions and the chemical potential of a proton, $E^{\text{offset}} = -H_p^{\text{QM}} + H_d^{\text{QM}} + \mu$. This result demonstrates that $E_{\text{EDS}}(1/s=1)$ yields the identical conformational ensemble to a SGC simulation at convergence.

If we assume a baseline EDS Hamiltonian enveloping deprotonated and protonated states without smoothing, $H_{\text{EDS}}(1/s=0) = \min(H_d(\mathbf{x}, \mathbf{p}), H_p(\mathbf{x}, \mathbf{p}))$, its partition function, $Z_{\text{EDS}}(1/s=0)$ can be written as follows:

$$Z_{\text{EDS}}(1/s=0) = \iint d\mathbf{x} d\mathbf{p} e^{-\beta \min[H_d(\mathbf{x}, \mathbf{p}), H_p(\mathbf{x}, \mathbf{p})]} \quad (20)$$

$$= \int d\mathbf{p} \left(\int_{R_d} e^{-\beta H_d(\mathbf{x}, \mathbf{p})} d\mathbf{x} + \int_{R_p} e^{-\beta H_p(\mathbf{x}, \mathbf{p})} d\mathbf{x} \right) \quad (21)$$

where R_d is the region where H_d has lower potential energy than H_p and H_p has lower potential energy in R_p . From the given $Z_{\text{EDS}}(1/s=0)$, the probability of sampling a conformation $\mathbf{x} \in R_d$ is

$$P(\mathbf{x}; 1/s=0) = \int d\mathbf{p} e^{-\beta \min[H_d(\mathbf{x}, \mathbf{p}), H_p(\mathbf{x}, \mathbf{p})]} / Z_{\text{EDS}}(1/s=0) \quad (22)$$

$$= \begin{cases} e^{-\beta E_d(\mathbf{x})} / Z'_{\text{EDS}} & \text{if } \mathbf{x} \in R_d \\ e^{-\beta[E_p(\mathbf{x}) - E^{\text{offset}}]} / Z'_{\text{EDS}} & \text{if } \mathbf{x} \in R_p \end{cases} \quad (23)$$

where $Z'_{\text{EDS}} = \int_{\mathbf{x} \in R_d} e^{-\beta E_d(\mathbf{x})} d\mathbf{x} + \int_{\mathbf{x} \in R_p} e^{-\beta[E_p(\mathbf{x}) - E^{\text{offset}}]} d\mathbf{x}$. It should be noted that eq 24 is not identical with eq 11, which indicates that the ensemble obtained by $H_{\text{EDS}}(1/s=0)$ is deviated from the SGC ensemble; however, this deviation can easily be accounted for by an on-the-fly reweighting scheme that we employ. It is well-known that the ensemble average $\langle A \rangle_0$ of some property A that is obtained from an energy function E_0 can be reproduced from the simulation of a different energy E_1 by considering the difference between two energies:⁵⁴

$$\langle A \rangle_0 = \frac{\langle A \exp[\beta(E_1 - E_0)] \rangle_1}{\langle \exp[\beta(E_1 - E_0)] \rangle_1} \quad (24)$$

Because we already know that $E_{\text{EDS}}(1/s=1)$ leads to the correct SGC ensemble, the SGC ensemble average of an observable A can be obtained from the simulation of $E_{\text{EDS}}(1/s=0)$ by considering the difference between two energy functions. Thus, for $\mathbf{x} \in R_d$, a reweighting factor $w(\mathbf{x} \in R_d) = \exp[\beta(E_{\text{EDS}}(1/s=0) - E_{\text{EDS}}(1/s=1))]$ is

$$w(\mathbf{x} \in R_d) = \exp[\beta(E_d + \beta^{-1} \ln(\exp(-\beta E_d) + \exp(-\beta E'_p)))] \quad (25)$$

$$= 1 + \exp[\beta(E_d - E'_p)] \quad (26)$$

where $E'_p = E_p - E^{\text{offset}}$. For $\mathbf{x} \in R_p$,

$$w(\mathbf{x} \in R_p) = 1 + \exp[\beta(E'_p - E_d)] \quad (27)$$

Using these weighting factors,

$$\langle A \rangle_{\text{EDS}} = \frac{\int A(\mathbf{x}) P(\mathbf{x}; 1/s=0) w(\mathbf{x}) d\mathbf{x}}{\int P(\mathbf{x}; 1/s=0) w(\mathbf{x}) d\mathbf{x}} \quad (28)$$

$$\begin{aligned} &= \frac{Z'^{-1} \left(\int_{R_d} A(\mathbf{x}) e^{-\beta E_d} (1 + e^{\beta(E_d - E'_p)}) + \int_{R_p} A(\mathbf{x}) e^{-\beta E'_p} (1 + e^{\beta(E'_p - E_d)}) \right)}{Z'^{-1} \left(\int_{R_d} e^{-\beta E_d} (1 + e^{\beta(E_d - E'_p)}) + \int_{R_p} e^{-\beta E'_p} (1 + e^{\beta(E'_p - E_d)}) \right)} \end{aligned} \quad (29)$$

$$= \frac{\int A(\mathbf{x}) (e^{-\beta E_d} + e^{-\beta E'_p})}{\int e^{-\beta E_d} + e^{-\beta E'_p}} \quad (30)$$

which suggests that our method can exactly reproduce the thermodynamic properties of the SGC ensemble with a proper reweighting using eqs 27 and 28, when simulating on the $1/s = 0$ surface.

In summary, we demonstrated that our method can successfully reproduce the thermodynamic quantities of the SGC ensemble at a given constant pH in two ways: (1) by performing MD simulation using $E_{\text{EDS}}(1/s=0)$ and on-the-fly reweighting the obtained conformations by using eqs 27 and 28 or (2) by performing MD simulation using $E_{\text{EDS}}(1/s=1)$. As pointed out by Christ and van Gunsteren,^{34,35,55} the reweighting schemes presented here do not suffer from the well-known numerical accuracy problems seen with other experimental reweighting schemes (e.g., thermodynamic integration), because with the EDS approach it is impossible to have a conformation where there is an exponent of a large positive number. Thus, the integration and its error bars are well-behaved. This is why the EDS approach is often optimal for connecting diverse surfaces.

2.1.3. pH-Dependent Offset Values. E^{offset} values are used to adjust the relative free energy differences between EDS end states.³³ To determine E^{offset} values for systems with a single titratable site (two end states), we rely on the known experimental pK_a values and thermodynamic integration calculations of a model compound. In this study, solvated amino acid monomers with capped termini were used as model compounds. Following Mongan et al.,¹⁸ it is assumed that the total protonation free energy consists of molecular mechanics (MM) and nonmolecular mechanics (non-MM) terms and that it has a linear relationship with external pH and an experimental pK_a value:

$$\Delta G_{\text{model}} = \Delta G_{\text{model}}^{\text{MM}} + \Delta G_{\text{model}}^{\text{non-MM}} \quad (32)$$

$$= k_B T \ln 10 (\text{pH} - pK_{a,\text{model}}) \quad (33)$$

With the assumption that the non-MM contribution of the model system is identical to that of a protein, ($\Delta G_{\text{protein}}^{\text{non-MM}} = \Delta G_{\text{model}}^{\text{non-MM}}$), the pH-dependent protonation free energy of a titratable group in a protein under a given pH condition can be calculated as

$$\begin{aligned} \Delta G_{\text{protein}} &= \Delta G_{\text{protein}}^{\text{MM}} + \Delta G_{\text{model}}^{\text{non-MM}} \\ &= \Delta G_{\text{protein}}^{\text{MM}} - \Delta G_{\text{model}}^{\text{MM}} + k_B T \ln 10 (\text{pH} - pK_{a,\text{model}}) \end{aligned} \quad (34)$$

This result clearly indicates that the SGC distribution of protonated and deprotonated states for a single titratable group can be obtained by running the EDS simulation with the following energy offset value:

$$E^{\text{offset}}(\text{pH}) = \Delta G_{\text{model}}^{\text{MM}} - k_B T \ln 10 (\text{pH} - pK_{a,\text{model}}) \quad (35)$$

The deprotonated state is taken as a reference state and its $E^{\text{offset}} = 0$, while $E^{\text{offset}}(\text{pH})$ is applied on protonated states. Note that, in contrast to the previous study, we set the deprotonated state as a reference state in this study.

The offsets $E^{\text{offset}}(\text{pH})$ depend on the type of the titratable group. For the simulation setup presented as follows, the $\Delta G_{\text{model}}^{\text{MM}}$ values have been determined by us previously through thermodynamic integration³³ and are shown in Table 1 together with the model compound pK_a values, i.e., $pK_{a,\text{model}}$.

In cases when multiple protonizable groups are permuted to titrate in a single EDS simulation, the reference state is the state in which all groups are deprotonated. For states which contain one protonated group, the offset is equal to $E^{\text{offset}}(\text{pH})$ in eq 35 and will depend on the type of the titratable group (see Table 1). For states in which multiple titratable groups are

Table 1. Experimental pK_a Values^{56,57} and Calculated Protonation Free Energy, $\Delta G_{\text{model}}^{\text{MM}}$ (from Equation 33) of Titratable Residues in Explicit Water Using the CHARMM22 Force Field⁵⁸

titratable residue	$pK_{a,\text{model}}$	$\Delta G_{\text{model}}^{\text{MM}}$ (kcal/mol)
Asp	4.0	43.60
Glu	4.4	46.15
Lys	10.4	-22.40
His- δ	6.5	4.39
His- ϵ	7.1	13.12

protonated, the offset is simply a sum of individual offset terms $E^{\text{offset}}(\text{pH})$ for each of the protonated groups.

2.1.4. Replica Exchange between Hamiltonians with Different Smoothness Values. In HREM, coordinates are exchanged between Hamiltonians that have different biasing potentials^{37,59-61} or differently scaled energy terms.^{36,62,63} Using a Metropolis-type exchange criterion yields the canonical ensembles of the given Hamiltonians in the ergodic limit. In many applications, HREM has been shown to be more efficient in conformational sampling than temperature exchange methods.^{36,37,45,59-64}

As mentioned previously, a small s value in the hybrid or EDS Hamiltonian given by eq 1 leads to a smoother energy landscape and lower energy barriers between states. However, aggressive smoothing of the energy landscape results in sampling of mostly nonphysical states. On the contrary, a large s value yields more physical ensembles, but energy barriers slow down the convergence of simulations. To solve this problem, we previously combined multiple EDS potentials with different smoothness parameters by using Hamiltonian replica exchange (HREM).³³ First, we generated an unsmoothed (baseline) Hamiltonian with $1/s = 0$ denoted H^0 to perform accurate conformational sampling. We have shown previously that this Hamiltonian follows the minimum energy surface among multiple end states.³³ The conformations sampled with H^0 correspond to one of the original end states, and we denote the corresponding ensemble Γ_0 .

In addition to the baseline Hamiltonian, smoothed Hamiltonians are generated and conformations are exchanged between them regularly to overcome high energy barriers in H^0 . To ensure the Boltzmann distribution of all Hamiltonians, the Metropolis-type exchange is utilized:

$$\begin{aligned} W(\mathbf{x}, s_m, \text{pH}; \mathbf{x}', s_n, \text{pH}) &= 1 & \text{if } \Delta \leq 0 \\ &= \exp(-\Delta) & \text{if } \Delta > 0 \end{aligned} \quad (36)$$

where s_m and s_n represent different smoothness parameters, \mathbf{x} and \mathbf{x}' are different coordinates, and

$$\begin{aligned} \Delta \equiv & \beta[(E_{\text{EDS}}(\mathbf{x}', s_m, \text{pH}) + E_{\text{EDS}}(\mathbf{x}, s_n, \text{pH})) \\ & - (E_{\text{EDS}}(\mathbf{x}, s_m, \text{pH}) + E_{\text{EDS}}(\mathbf{x}', s_n, \text{pH}))] \end{aligned} \quad (37)$$

Thus, if exchanges are performed between different EDS potentials based on eq 36, the resulting Γ_0 will correspond to a precise SGC ensemble of multiple protonation states at a given pH.

2.2. Two-Dimensional Replica Exchange. In this study, we devised a two-dimensional Hamiltonian replica exchange method. Hamiltonian exchanges are performed not only between EDS potentials but also between different pH conditions. The different pH conditions are represented by

adjusting the offsets between the end states; unlike prior discrete-state pH replica exchange methods,^{24,28,65} it is not necessary to devise a new criterion for exchanges between replicas at different pH values. This is because all titration states are simulated simultaneously via the hybrid Hamiltonian. Therefore, exchanges between pH values use the normal Hamiltonian exchange criterion described as follows:

$$W(\mathbf{x}, s, \text{pH}_i; \mathbf{x}', s, \text{pH}_j) = 1 \quad \text{if } \Delta \leq 0 \quad (38)$$

$$= \exp(-\Delta) \quad \text{if } \Delta > 0 \quad (39)$$

where pH_i and pH_j represent different pH values, \mathbf{x} and \mathbf{x}' are different coordinates, and the smoothness parameter s is constant:

$$\Delta \equiv \beta[(E_{\text{EDS}}(\mathbf{x}', s, \text{pH}_i) + E_{\text{EDS}}(\mathbf{x}, s, \text{pH}_j)) - (E_{\text{EDS}}(\mathbf{x}, s, \text{pH}_i) + E_{\text{EDS}}(\mathbf{x}', s, \text{pH}_j))] \quad (40)$$

The two-dimensional replica exchange setup is schematically represented in Figure 2. With the current implementation of

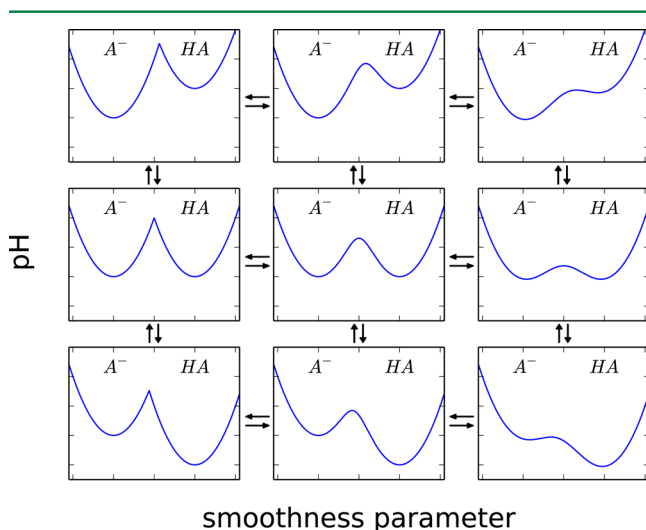


Figure 2. Schematic representation of a constant-pH simulation with the two-dimensional EDS-HREM method. The x-axis corresponds to the change of smoothness parameter, and the y-axis corresponds to the change of solution pH. The leftmost potentials are baseline Hamiltonians with $1/s = 0$. The arrows indicate that replica exchanges are performed between neighboring potentials.

the 2D exchange scheme, exchange attempts in each dimension are restricted between neighboring replicas. The effect of external pH is considered by adjusting the energy offset of a protonated state using the procedure described previously, while setting the offset of the completely deprotonated state to zero.

We implemented this 2D exchange scheme into the REPDSTR facility⁶⁶ in CHARMM.⁶⁷ The 2D code is not limited to EDS constant-pH simulations. Two-dimensional exchanges may be performed between any types of Hamiltonians. Furthermore, because the definition of each dimension is flexible, the 2D exchange command can perform other types of two-dimensional exchange simulations, such as temperature–Hamiltonian exchange and SGLD replica exchange.^{68,69}

2.3. Preparing Initial Structures. Five systems were used to assess the performance of the 2D exchange method: aspartic

acid, glutamic acid, and lysine monomers, a four residue peptide with sequence KAAE, and snake cardiotoxin V from *Naja naja atra* (CTX AS, Protein Data Bank (PDB) ID: 1CVO).⁷⁰ The initial structures of all test systems were generated by the CHARMMing server⁷¹ with the CHARMM22 parameters.⁵⁸ The N- and C-termini of all systems were capped with the neutral acetyl and N-methyl groups. The amino acid monomers and the KAAE peptide were solvated in 30 Å cubic boxes, and the snake cardiotoxin was solvated in a 60 Å cubic box. The TIP3P water model⁷² was employed in all cases. All initial structures were energy-minimized by 200 steps of steepest descent followed by 200 steps of the adopted basis Newton–Raphson method.⁷³ After minimization, the systems were equilibrated with a constant pressure of 1 atm for 1 ns.

In this study, the change of protonation state was modeled by the change of partial charges of side chains. Therefore, the deprotonated states have a dummy hydrogen atom with zero charge, while keeping the bond, angle, and van der Waals (vdW) interactions constant. The contributions of these terms cancel out under the assumption that the non-MM free energy components of the model compound and target system are the same. However, it should be noted that this assumption has a limitation. As discussed by Bürgi et al.,¹⁷ the vdW parameters of atoms in general may vary in different protonation states, and their contribution to the free energy of protonation may be comparable to the electrostatic contribution. Thus, the current study is missing the effect of the change of vdW parameters. However, in principle, the MSCALE module allows the consideration of this effect by changing the vdW parameters of the subsystems.

The charges of titratable groups were adopted from the CHARMM22 parameter set.¹⁹

2.4. Two-Dimensional EDS-HREM Simulations. All calculations in this study were performed with the EDS command⁷⁴ of CHARMM's MSCALE facility.⁷⁵ MSCALE allows the user to define different subsystems and then combines the energy and forces of them in a configurable manner. In this study, each subsystem represents a specific protonation state. In the main process, the hybrid EDS potential energy and forces, incorporating the inputs from each subsystem, are calculated based on eq 1 and are used for Verlet integration. Offset values for EDS were assigned in accordance to the values from Table 1 and the simulation pH.

For all simulations, replica exchanges between EDS Hamiltonians and different pH conditions were attempted every 100 steps, alternating between exchanging EDS s values and pH values. A time step of 1 fs was used and the Nose–Hoover thermostat^{76,77} was employed to maintain a temperature of 300 K. The SHAKE algorithm constrained the length of bonds involving hydrogen atoms to their parameter set values. The cutoff used for building the nonbonded list was 15 Å. Electrostatic interactions were truncated by the force shift method with a cutoff of 12 Å, and the Lennard-Jones interactions were truncated with a switching function between 10 and 12 Å. Note that the Ewald or particle mesh Ewald methods were not used because the net charge of the system varies.⁷⁸ The last snapshots of the equilibration runs were used as the initial structure for the molecular dynamics simulations, which were performed under constant volume conditions.

For EDS-HREM simulations, s values were spaced so as to yield an average exchange rate greater than 20%. A total of four EDS potentials with $1/s$ values of 0, 36.6, 50.0, and 100.0 were used for the simulations of amino acid monomers. For the

KAAE peptide, four EDS potentials with $1/s$ values of 0, 36.6, 47.6, and 62.5 were used. Six potentials were used for snake cardiotoxin with $1/s$ values of 0, 30.3, 37.0, 45.5, 55.6, and 100.0.

2.5. Calculation of pK_a Values. pK_a values from the simulations were determined by fitting the deprotonated fractions from the baseline Hamiltonians sampled at different pH values to the Hill equation:

$$f(\text{pH}) = \frac{1}{1 + 10^{n(\text{pH} - \text{pH}_a)}} \quad (41)$$

where $f(\text{pH})$ is the fraction of the deprotonated state at a given pH and n is the Hill coefficient.

The f value of the j th titratable residue, $f^{(j)}$, can be calculated from the sum of the fractions of states where the j th residue is in the deprotonated state. This can be readily obtained by using eq 16 as follows:

$$f^{(j)}(\Gamma^0) = \frac{1}{N} \sum_{i=1}^N \frac{\sum_{\mathbf{n}} n_j e^{-\beta[E(\mathbf{x}_i, \mathbf{n}) - E^{\text{offset}}(\mathbf{n})]}}{\sum_{\mathbf{n}} e^{-\beta[E(\mathbf{x}_i, \mathbf{n}) - E^{\text{offset}}(\mathbf{n})]}} \quad (42)$$

where N is the number of configurations in Γ^0 , $\mathbf{x}_i \in \Gamma^0$, \mathbf{n} is a protonation-state vector where $n_j = 1$ if the j th residue is deprotonated and otherwise $n_j = 0$, $E(\mathbf{x}_i, \mathbf{n})$ is the potential energy of a protonation state \mathbf{n} at a conformation \mathbf{x}_i , and $E^{\text{offset}}(\mathbf{n})$ is the offset energy of the protonation state \mathbf{n} .

Fitting deprotonated fractions to the Hill equation was performed by the linear and nonlinear mixed effects (NLME) modules^{79–81} of the R package.⁸²

2.6. Calculation of Transition Rates. The speed of convergence of any replica exchange simulation, regardless of its dimension, depends on the speed of sampling of the replica that explores conformation states the fastest.⁸³ This fact has led to the development of both Boltzmann and non-Boltzmann reservoir replica exchange methods, which attempt to separate conformational search from state space sampling.^{84–86} EDS-HREM was not coupled to a reservoir in this study, which means that all exploration of conformational space and protonation states must be accomplished within the dynamics simulation. Therefore, it is critical to understand whether allowing replicas to exchange between pH values in addition to EDS Hamiltonians enhances this process. One method to do so is to simply count the number of times a given simulation changes its titration state. Recall that transitions between end states imply a change in protonation state for one or possibly multiple titratable groups. In this study, we assigned the protonation state of a conformation \mathbf{x} based on the state probability defined by eq 16. If $P(\mathbf{x}, \mathbf{n}) > 0.9999$, \mathbf{x} is considered to be in the protonation state \mathbf{n} . Otherwise, it is considered to be in an intermediate state.

Two obvious methods for counting protonation-state transitions at base ($1/s = 0$) replicas can be considered. The most straightforward is to simply count every change in state, regardless of whether it occurred as the result of a replica exchange move or dynamics step move, as a transition (Figure 3B). We call these *apparent* transitions, for reasons given later. The other method, used in our prior work,³³ is to follow the state trace of a replica as it switches between Hamiltonians with different s values and count only switches between different states that occur during dynamics. In order to fully undergo a state transition, a replica must start at a baseline Hamiltonian at any pH, transition during dynamics to a different state, and

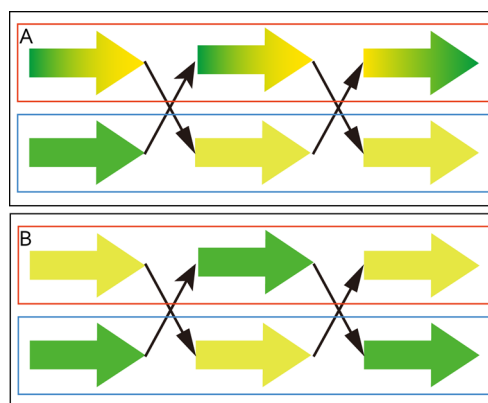


Figure 3. Schematic representation of (A) actual and (B) apparent transitions. Thick arrows represent MD simulations of a replica, and thin black arrows represent the exchanges of replicas between different EDS potentials. Green and yellow colors indicate two different protonation states. Red and blue boxes correspond to smoothed and baseline EDS potentials, respectively. (A) In the actual transitions, the change of protonation state occurs during the MD simulation due to lowered energy barriers in the smoothed EDS potential. (B) In the apparent transitions, the two protonation states are sampled in the baseline EDS potential without crossing energy barriers due to replica exchanges.

then return to a baseline Hamiltonian at any other pH. This indicates that the replica has actually crossed an energy barrier and sampled the transition regions although possibly in a highly smoothed replica. We call these *actual* transitions (Figure 3A).

To illustrate why actual transitions govern correct sampling during a 1D or 2D EDS-HREM simulation, consider a simplified system with only two replicas, where each replica may exist in one of two conformations that are approximately equal in free energy but separated by a high barrier that is constant between the replicas. Suppose further that one replica is started in each conformation and that exchanges are attempted regularly. Since the two conformations have approximately equal free energy, frequent exchanges will occur, meaning that there will be a large number of apparent transitions. However, with a high barrier, there will be few, if any, transitions occurring during the dynamics (i.e., actual transitions). Therefore, although it may appear that the system switches between states regularly, in fact, the barrier region remains poorly sampled and the assumption of constant-pH methods that the free energy between conformations is adequately determined fails to hold.

For the purpose of this work, all pH state transition numbers reported are actual transitions.

2.7. Conformational Clustering Analysis. Since pH and conformation states may be closely related,^{87–89} we investigated whether different conformations were explored during 2D EDS-HREM simulations. To assess the efficiency of conformational sampling, clustering of baseline trajectories was carried out by using the ART-2' algorithm⁹⁰ implemented in CHARMM⁶⁷ using the CLUSTER subcommand of the CORREL module.

In the ART-2' algorithm, each conformation is represented by a N -dimensional vector $\mathbf{x} = (x_1, x_2, \dots, x_N)$ and a cluster is defined by its cluster center, \mathbf{C}_k , the average of all conformations in the cluster; that is,

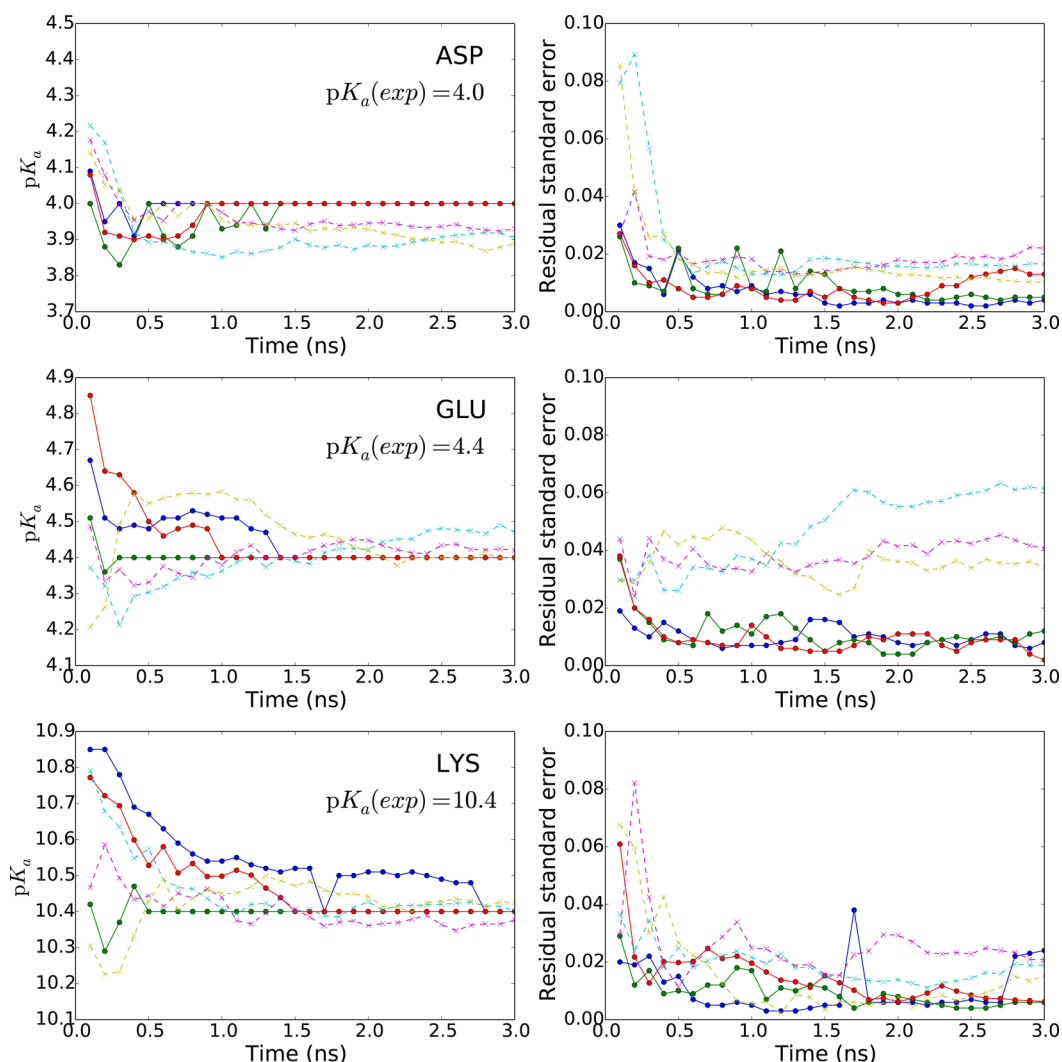


Figure 4. Time series of calculated pK_a values (left) and residual standard errors (right) of amino acid monomers obtained by three independent simulations using the 1D (dotted lines) and 2D (solid lines) EDS-HREM methods. Three amino acid monomers are used: aspartic acid (top), glutamic acid (middle), and lysine (bottom).

$$C_k = \frac{1}{M} \sum_{\mathbf{x}_j \in C_k} \mathbf{x}_j \quad (43)$$

where M is the number of conformations in the cluster. The distance between a conformation \mathbf{x}_i and a cluster center C_k is defined by the Euclidean distance:

$$d_{ik} = \sqrt{\frac{\sum_{j=1}^N |x_{i,j} - C_{k,j}|^2}{N}} \quad (44)$$

where $x_{i,j}$ and $C_{k,j}$ are the j th component of \mathbf{x}_i and C_k . For the initial round of the clustering, the first conformation in a trajectory becomes the center of the first cluster (Supporting Information Figures S2A and S3A). If the second conformation is within a preset distance cutoff, it is also assigned to the first cluster. Otherwise, it forms the center of a second cluster (Supporting Information Figures S2B and S3B). This procedure is repeated for all structures in the trajectory (Supporting Information Figure S2C and S3C). After this first round of clustering, the centers of clusters are recalculated to minimize the sum of Euclidean distances between the centers and their members, and the membership of each conformation

is reassigned based on the newly obtained cluster centers (Supporting Information Figure S2D and S3D). Note that the number of clusters can be changed during this refinement step, meaning that the number of clusters is not known a priori and is dynamically determined by the extent of sampled conformations. The refinement procedure is performed iteratively to minimize the sum of distances between the cluster center and its associated members under the cluster radius constraint, which states that the distances between the cluster center and all of its members are less than the threshold.^{91,92}

In this study, the backbone ϕ and ψ angles of proteins were used to represent a conformation. A distance cutoff of 20° was used for the KAAE peptide and snake cardiotoxin. Because the algorithm depends on the ordering of frames, we randomly shuffled the time series of backbone ϕ/ψ angles 10 times and calculated the average and standard deviations of the number of clusters. Because the radius of each cluster is the same, the number of clusters represents the amount of sampling in backbone dihedral space.

3. RESULTS AND DISCUSSION

3.1. Two-State Systems. To assess the improvement of 2D replica exchange over 1D replica exchange, we performed constant-pH simulations of three amino acid monomers: aspartic acid, glutamic acid, and lysine. All constant-pH MD simulations were performed for 3 ns with both 1D and 2D EDS-HREM. For all amino acids, constant-pH simulations were performed at five different pH values centered at the experimental pK_a of the target amino acid and spaced in increments of 1 pH unit. For each simulated pH value, the deprotonated fractions $f_i(\tau)$ were calculated as a function of simulation time τ (or equivalently as a function of the number of configurations sampled from time $t = 0$ until time $t = \tau$). Here i is an index over $N_{\text{pH}} = 5$ pH values. The $pK_a(\tau)$ values and residual standard errors $\hat{\sigma}(\tau)$ at each time step were determined by fitting $f_i(\tau)$ values to the Hill equation (eq 41). The residual standard errors are defined as

$$\hat{\sigma}(\tau) = \sqrt{\frac{\sum_{i=1}^{N_{\text{pH}}} \hat{f}_i(\tau) - f_i(\tau)}{N_{\text{pH}} - 2}} \quad (45)$$

Here $\hat{f}_i(\tau)$ is the deprotonated fraction that would correspond to a point on the fitted titration curve. The time series of calculated $pK_a(\tau)$ and $\sigma(\tau)$ values are shown in Figure 4.

These results show that the calculated $pK_a(\tau)$ values of most of the 2D replica exchange simulations converge to the experimental value within $\tau = 1.5$ ns. On the contrary, the three $pK_a(\tau)$ values from the 1D simulations deviate from the experimental value and from each other during the entire 3.0 ns run, suggesting that the convergence rate of 2D simulations is significantly faster than that of 1D simulations. The residual standard error results also support this conclusion. The errors obtained from 2D simulations are consistently lower than those of 1D simulations for 3 ns.

The efficiency of constant-pH simulation is tied to the number of actual protonation-state transitions of each replica as described earlier. A comparison of the number of protonation-state transitions per 1 ns by the 1D and 2D EDS-HREM is given in Table 2. The values in the table are the averages over

Table 2. Average Number of Protonation-State Transitions with 1D and 2D Replica Exchange Methods for 1 ns

ASP	GLU			LYS		
	pH	2D	1D	pH	2D	1D
2	22.0	4.7	2.4	22.8	4.7	8.4
3	32.2	12.7	3.4	24.2	17.1	9.4
4	23.8	34.8	4.4	25.8	33.5	10.4
5	24.2	26.5	5.4	23.9	29.6	11.4
6	25.0	6.2	6.4	23.7	9.0	12.4
av	26.2	17.0		24.1	18.8	24.0

three independent simulations at each pH. The results show that, compared to the 1D method, the 2D EDS-HREM method increases the number of actual transitions by about 46%.

More importantly, the 2D method increases the number of transitions by a factor of 2–4 at pH values that are further away from the pK_a value. The small number of transitions at extreme pH values for 1D EDS-HREM significantly slows down the convergence of pK_a estimates. However, with the 2D method, all replicas show similar numbers of actual transitions due to frequent exchanges between different pH conditions. In other

words, in the 2D simulation, the memory of the initial pH condition becomes lost rapidly. The larger number of transitions at extreme pH conditions leads to faster convergence and a more accurate fitting result. These results demonstrate that coupling simulations at different pH conditions through exchanges can enhance the sampling efficiency significantly, as was previously demonstrated in earlier pH replica exchange simulations.²⁴

The number of transitions observed in this study is comparable to other constant-pH simulations in explicit solvent. During the 1 ns simulations of amino acids, the average number of actual protonation-state transitions from the 2D EDS-HREM method ranges from 24.0 to 26.2 (Table 2). Goh et al.²⁷ achieved ~50 transitions per ns for the titrations of adenine and cytosine, and Donnini et al.²⁶ reported ~100 transitions during 20 ns of the constant-pH simulation of imidazole, which corresponds to ~5 transitions per ns. It should be noted that when multiple residues are titrated, our method can sample the simultaneous protonation-state transitions of these residues.

3.2. KAAE Peptide. The KAAE peptide can adopt four possible protonation states because it has two titratable groups: Lys-1 and Glu-4. We performed three independent constant-pH simulations of it at six pH values from 2.4 to 12.4 in an interval of 2 pH units using the 1D and 2D EDS-HREM methods. The titration curves and corresponding pK_a values and Hill coefficients were estimated by fitting the average deprotonated fraction at each pH to the Hill equation (eq 41).

Figure 5 shows the fitted titration curves from the 1D and 2D simulations. It shows that the residual standard error from the 2D simulations (0.034) is smaller than that from the 1D simulations (0.046), although both errors are small. In addition, the standard deviations of the deprotonated fraction from the 2D simulations are smaller than those from the 1D simulations except at pH = 6.4, where the standard deviations with the 2D method is only slightly larger.

The calculated pK_a shifts of Lys-1 and Glu-4 from the 1D and 2D simulations show little difference. The calculated pK_a value of Lys-1 is larger than the model compound pK_a value, while that of Glu-4 is slightly smaller. These shifts mean that, compared to the model compound, the charged states of both residues are favored over the neutral states due to the electrostatic interaction between two residues.

To quantify how much the 2D EDS-HREM method enhances simulation convergence in terms of simulation time, we counted the number of actual protonation-state transitions at each pH (Table 3). The table shows that on average using the 2D method increases the number of actual transitions by 65% over the 1D EDS-HREM, but the increase is considerably larger at pH values that are further away from the pK_a values, which is similar to the results from the amino acid monomers. For example, at pH = 8.4, the number of transitions increased 8.8-fold from 1.7 to 15.0. When the 1D method is used, more frequent actual transitions than the 2D method are observed only at the pH conditions close to the pK_a values of glutamic acid and lysine, 4.4 and 12.4. The smaller numbers of transitions by the 2D method at these pH values appear to be caused by the re-distribution of transitions to other pH values.

For this system, the protonation state of a titratable group is tightly coupled with its conformation. Based on the molecular mechanics (MM) model, protonation states are determined by electrostatic interactions, which are orthogonal to the effects of

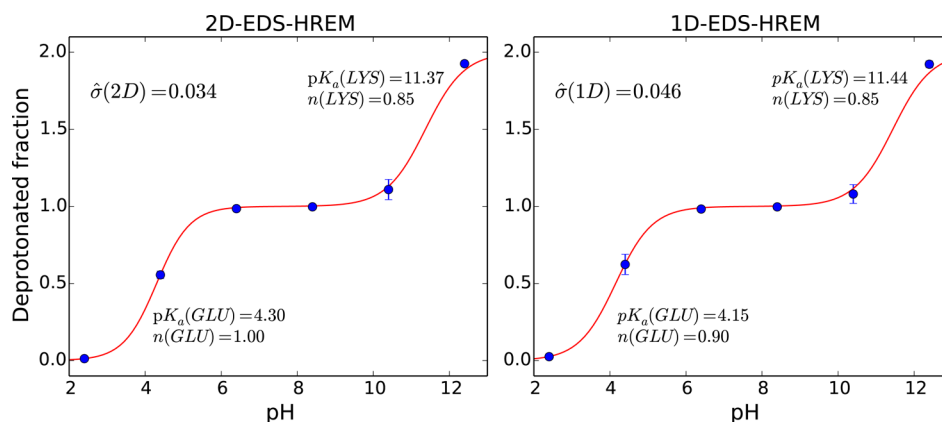


Figure 5. Titration curves of the KAAE peptide obtained from three 1 ns constant-pH simulations using the 2D (left) and 1D (right) EDS-HREM methods. Solid lines are fitted Hill equation curves. Blue dots and error bars represent the average and standard deviations of deprotonated fractions. The residual standard error ($\hat{\sigma}$) of fitting is shown at top left. The calculated pK_a values and Hill coefficients of glutamic acid and lysine are shown at bottom left.

Table 3. Comparison of the Number of Actual Protonation-State Transitions of KAAE Peptide with the 1D and 2D EDS-HREM Methods^a

initial pH	no. of transitions	
	2D REM	1D REM
2.4	14.7 (5.0)	5.5 (1.9)
4.4	16.0 (4.6)	20.9 (6.7)
6.4	20.0 (4.1)	4.0 (1.5)
8.4	15.0 (2.9)	1.7 (0.6)
10.4	11.3 (4.6)	6.9 (2.7)
12.4	13.0 (4.6)	15.5 (4.5)
av	15.0 (5.1)	9.1 (3.6)

^aNote that both lysine and glutamic acid are titratable and a transition between any pair of protonation states is counted. Standard deviations are shown in parentheses.

other energy terms such as van der Waals or dihedral angles. It is essential to achieve a diverse conformational state sampling by overcoming these hidden barriers for an accurate constant-pH simulation. Hence, one can ask whether the 2D method can enhance conformational sampling as well as protonation-state transitions.

We performed a clustering analysis of the ensembles from the 1D and 2D EDS-HREM simulations using the ART-2' algorithm.⁹⁰ For each cluster, all conformations are within a distance threshold, 20° , from the center of the cluster, and the number of clusters are not known a priori. Thus, the number of clusters is a proxy that represents the extent of conformational sampling. From Table 4, it is apparent that the 2D EDS-HREM method facilitates more diverse conformational sampling than the 1D method. Using 2D EDS-HREM increases the number of clusters sampled by 59% on average. The only case where 1D comes close to 2D is at pH = 12.4. Since the pK_a of Lys-1 is 12.4, even the 1D simulation experiences frequent transitions.

3.3. Snake Cardiotoxin. Two-dimensional EDS-HREM also has an advantage on more complex systems such as snake cardiotoxin (CTX A5, PDB ID: 1CVO).⁷⁰ Snake cardiotoxin has 14 titratable groups, but only three, Glu-17, Asp-42, and Asp-59, are titratable in the pH range between 2 and 5.^{46,47} Including these three titratable residues results in eight possible protonation states. Three sets of 1D and 2D EDS-HREM constant-pH simulations were performed at pH values ranging

Table 4. Average Number of Conformational Clusters of the KAAE Peptide from Three Independent 1D and 2D EDS-HREM Simulations^a

initial pH	no. of clusters	
	2D EDS-HREM	1D EDS-HREM
2.4	66.4 (10.6)	44.0 (6.8)
4.4	86.3 (6.6)	41.7 (7.5)
6.4	79.2 (10.3)	56.6 (12.6)
8.4	78.5 (8.9)	42.5 (5.3)
10.4	77.0 (7.2)	38.5 (11.3)
12.4	55.3 (8.2)	55.8 (3.9)
av	73.8 (13.4)	46.5 (11.0)

^aStandard deviations are shown in parentheses.

from 1 to 5 in steps of 1 pH unit for 1 ns. All results were obtained from the average of three sets of simulations.

Figure 6 demonstrates that the 2D method yields significantly smaller standard deviations of deprotonated fractions than the 1D method. Considering the same simulation lengths of the 1D and 2D results, this indicates that the 2D method converges significantly faster than the 1D method. The most noticeable difference is between the titration curves of residue D42. The average deprotonated fractions from the 2D simulations closely lie on the titration curves for all pH values and have small error bars, while those from the 1D simulations at pH = 2, 3, and 4 are offset and have much larger error bars. The results of D59 show similar patterns. Although the average deprotonated fractions from the 1D and 2D simulations agree well with the fitted curves, the error bars from the 1D simulations are significantly larger than those from the 2D simulations. The results for E17 are relatively invariant to method because it is almost fully solvent exposed, which makes an extensive conformational sampling of this residue easier.

The calculated pK_a values from the 1D and 2D simulations are similar despite the significant difference in the convergence speed of the two methods. This is likely because both the 1D and 2D EDS-HREM simulations appear to be converged. The calculated pK_a values of D42 and D59 are in good agreement with the experimental values of 3.2 and less than 2.3, respectively.⁴⁷ The largest error is observed in E17, whose calculated pK_a value, 2.41, is much lower than the experimental pK_a value, 4.0. Considering that Glu-17 is the most converged

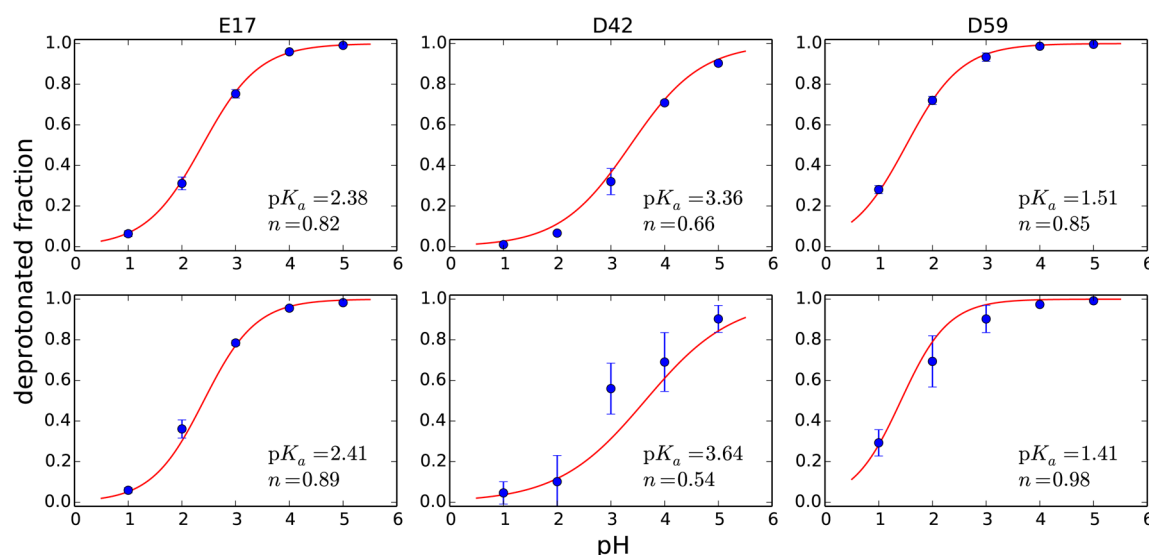


Figure 6. Fitted titration curves for the three titratable groups of snake cardiotoxin, Glu-17 (left), Asp-42 (middle), and Asp-59 (right), obtained with the 2D (upper panels) and 1D (lower panels) EDS-HREM methods. Solid red lines are fitted Hill equation curves. Blue dots and error bars represent the average standard deviations of deprotonated fractions from three independent 1 ns constant-pH EDS-HREM simulations at each pH condition.

among the three titratable groups in terms of sampling, this error may be caused for the following reasons. First, the fixed partial charge representation of E17 may not be enough. There are three positively charged residues, K2, K13, and K19 located near E17, and they interact with E17. If these interactions overstabilize the deprotonated state of E17, this may lead to a lowered pK_a estimation. Another source of error may be related to a net-charge problem. In this study, the net charge of the unit cell is nonzero. Recently, it was reported that conserving the net charge of the system by simultaneous change of counterions or water molecules could lead to more accurate pK_a estimation.⁶⁵ More detailed discussion can be found in our previous work.³³

We compared the number of protonation-state transitions obtained with the 1D and 2D EDS-HREM methods (Table 5).

Table 5. Average Number of Protonation-State Transitions of Snake Cardiotoxin by 1D and 2D Replica Exchange Schemes

initial pH	no. of transitions	
	2D REM	1D REM
1	22.0 (3.9)	13.2 (4.8)
2	17.6 (5.1)	18.8 (4.7)
3	18.3 (4.6)	14.7 (2.7)
4	16.5 (2.3)	9.7 (5.1)
5	14.7 (3.0)	5.0 (3.2)
av	17.8 (4.6)	12.3 (6.3)

On average, the 2D EDS-HREM method showed 46% more transitions than the 1D EDS-HREM method: from 12.2 to 17.8 transitions/ns. As in previous benchmark systems, the numbers of transitions with the 2D method are similar regardless of pH. However, with the 1D method, the number of transitions significantly decreases at extreme pHs, for which the observed number of actual transitions is about 2–3 times higher with the 2D method.

To get a more detailed view on how the 2D method enhances state transitions, we enumerated the number of

transitions of replicas started at pH = 2. In Figure 7, the state transitions are depicted by arrows whose widths are proportional to the number of transitions. The figure shows that the 2D method samples more diverse state transitions than the 1D method. With the 1D method, the most frequently observed transitions are between the PPD and DPD states. The average number of transitions per nanosecond from PPD to DPD is 3.0 and the reverse transition has a rate of 2.8 transitions/ns. The most frequent transition obtained with the 2D method is from the PPD to DPD state (2.27 times/ns), and the second most frequent transition is from the PPP to PPD state (1.97 times/ns). In addition, some transitions that involve the protonation-state changes of multiple residues, such as those from PPP to DDD and from PPD to DDD, were not sampled with the 1D method but are observed with the 2D method. This suggests that the 2D method allows for sampling of larger energy barriers than the 1D method. In summary, these results clearly show that 2D EDS-HREM enhances the number of actual protonation-state transitions.

It is worth noting that if there is no protonation-state transition at a particular pH, the estimated error for that pH will be zero. This is not a serious problem because the complete lack of transitions indicates that there is a dominantly sampled state with much lower free energy than any other state. If a simulation is initiated in such a way that a replica is trapped in a protonation state with higher free energy, the 2D method offers a much greater chance of escaping that state than the prior 1D method. In a 2D simulation, protonation-state transitions occur by crossing energy barriers or by replica exchange between different pH conditions; this significantly enhances the likelihood of transitioning out of an unfavorable starting state as compared to a 1D simulation (see Figure 7).

Does an enhanced number of protonation-state transitions indicate enhanced conformational sampling? To answer this question, we carried out a cluster analysis of ensembles from the 1D and 2D EDS-HREM simulations. The average numbers of conformational clusters sampled for 1 ns with the 1D and 2D EDS-HREM methods are listed in Table 6. When using the 2D method, the average number of conformational clusters

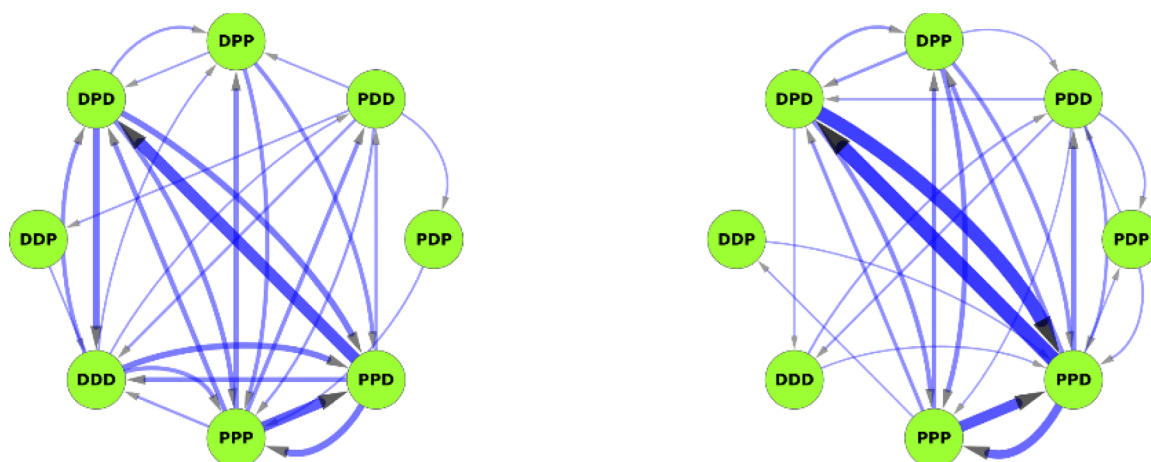


Figure 7. Illustrations of the average numbers of protonation-state transitions between eight possible states of snake cardiotoxin obtained with 1D (right) and 2D (left) EDS-HREM simulations started at pH = 2. P and D represent protonated and deprotonated states, respectively. The first, second, and third symbols correspond to Glu-17, Asp-42, and Asp-59. The width of the line is proportional to the number of transitions.

Table 6. Number of Conformational Clusters of Snake Cardiotoxin Sampled with the 1D and 2D EDS-HREM Constant-pH Methods^a

initial pH	no. of clusters	
	2D EDS-HREM	1D EDS-HREM
1	17.5 (3.3)	5.6 (2.3)
2	20.8 (4.5)	5.5 (2.5)
3	23.1 (1.7)	7.8 (3.8)
4	19.3 (2.6)	5.9 (2.8)
5	18.4 (2.3)	5.8 (2.2)
av	19.8 (3.6)	6.1 (2.9)

^aStandard deviations are shown in parentheses.

increases from 6.1 to 19.8. This difference can be also identified visually by looking at the superimposed trajectories of the 1D and 2D simulations (Figure 8). Overall, the 2D simulation

trajectory shows larger fluctuations. The difference is more noticeable in the loop regions, and the side chains of D42 and D59 are more widely spread in the 2D simulation. To check whether enhanced conformational sampling observed at individual pH values is not simply a consequence of redistribution of sampled conformations, we combined the trajectories from the five pH conditions into one and performed the clustering analysis using the merged trajectory. The average number of conformational clusters from the 2D simulations, 33.3, is almost twice that from the 1D simulations, 17.7. The increase in the number of clusters indicates that 2D EDS-HREM enhances the conformational sampling of constant-pH simulations of the combined trajectory.

In addition to the clustering analysis, we compared the root-mean-square fluctuation (RMSF) of each residue from the 1D and 2D simulations. Figure 9 shows that, for all pH conditions, the RMSF values of the 2D simulations are consistently larger

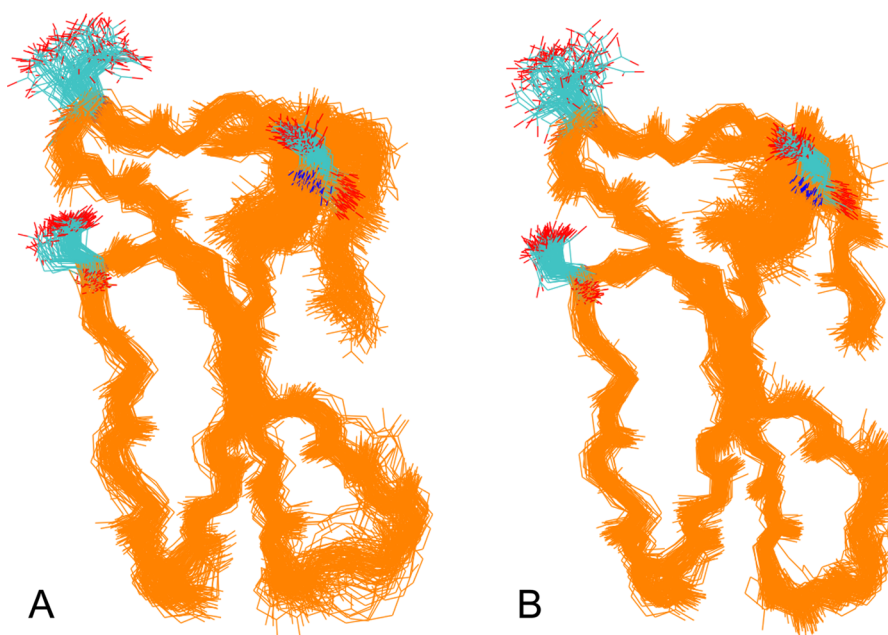


Figure 8. Superimposed 1 ns trajectories of snake cardiotoxin from the (A) 2D and (B) 1D constant-pH EDS-HREM simulations at pH = 2. Backbone structures are colored in orange, and three titratable groups are colored by atom.

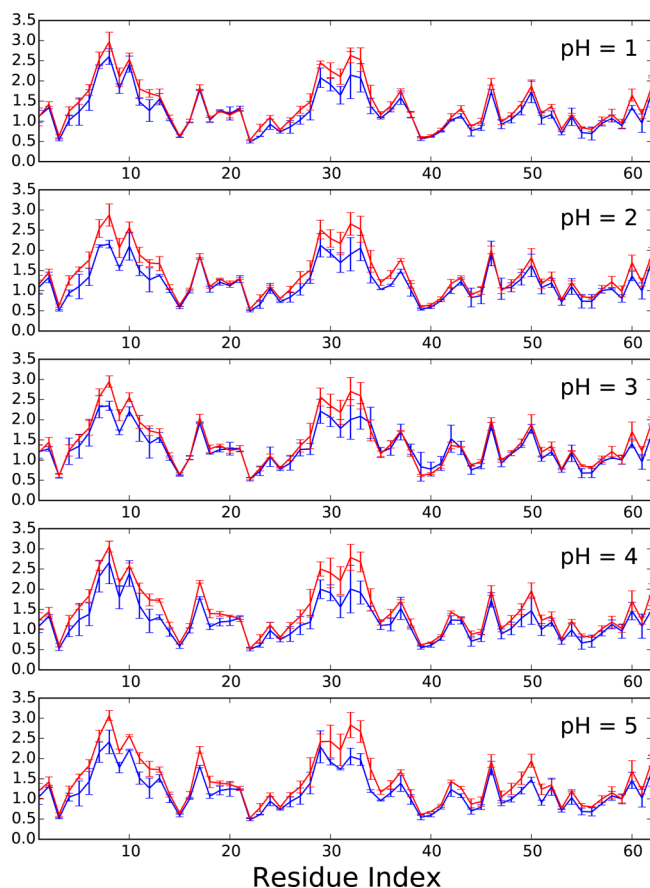


Figure 9. Residue RMSF plots obtained from the 2D (red) and 1D (blue) constant-pH simulations of snake cardiotoxin at pH values from 1 (top) to 5 (bottom). The standard deviations are calculated from three independent simulations.

than those of the 1D simulations throughout all residues. This result also demonstrates that the 2D simulation facilitates conformational sampling.

To get a more detailed view on the conformational sampling of titratable groups, we investigated the change of χ_1 angles of titratable groups at pH = 2 (Figure 10). Generally, the χ_1 angles can adopt three rotamer states: gauche(+), gauche(−), and trans. The figure shows that all three independent 2D simulations sample frequent transitions between gauche(+) and trans states of D42 and D59 from the beginning of the simulation. However, only a few state transitions of the χ_1 angle of D42 are observed with the 1D method and the gauche(−) state of D59 is sampled only once throughout the 3 ns trajectories obtained from this method. Additionally, the gauche(−) states of D42 is only observed with the 2D method. E17 shows more transitions than D42 and D59 because E17 is almost fully exposed to the solvent. However, it can be clearly identified that the sampling of the χ_1 angle of E17 is also enhanced with the 2D method. A rapid transition between the gauche(−) and trans states is observed with the 2D method at both conditions, while the same transition happens more slowly with the 1D method. The trends are qualitatively similar at all pH conditions. All of these results clearly demonstrate that the 2D method significantly enhances the conformational sampling and helps to overcome orthogonal energy barriers to the electrostatic interactions, such as dihedral angle energy.

4. CONCLUSIONS

In this study, we present the 2D EDS-HREM method for constant-pH simulations with explicit solvent. We show that the 2D method significantly outperforms the 1D EDS-HREM method in terms of convergence rate. For all benchmark systems, amino acid monomers, the KAAE peptide, and snake cardiotoxin, the average number of actual protonation-state transitions increases when using the 2D EDS-HREM method instead of the 1D method. For amino acid monomers, the calculated pK_a values obtained with the 1D method do not converge to the ideal value within 3 ns, and furthermore simulations started from different initial velocities differ slightly from the experiment. In contrast, with the 2D method the pK_a values from all simulations converge to the ideal value in 1.5 ns.

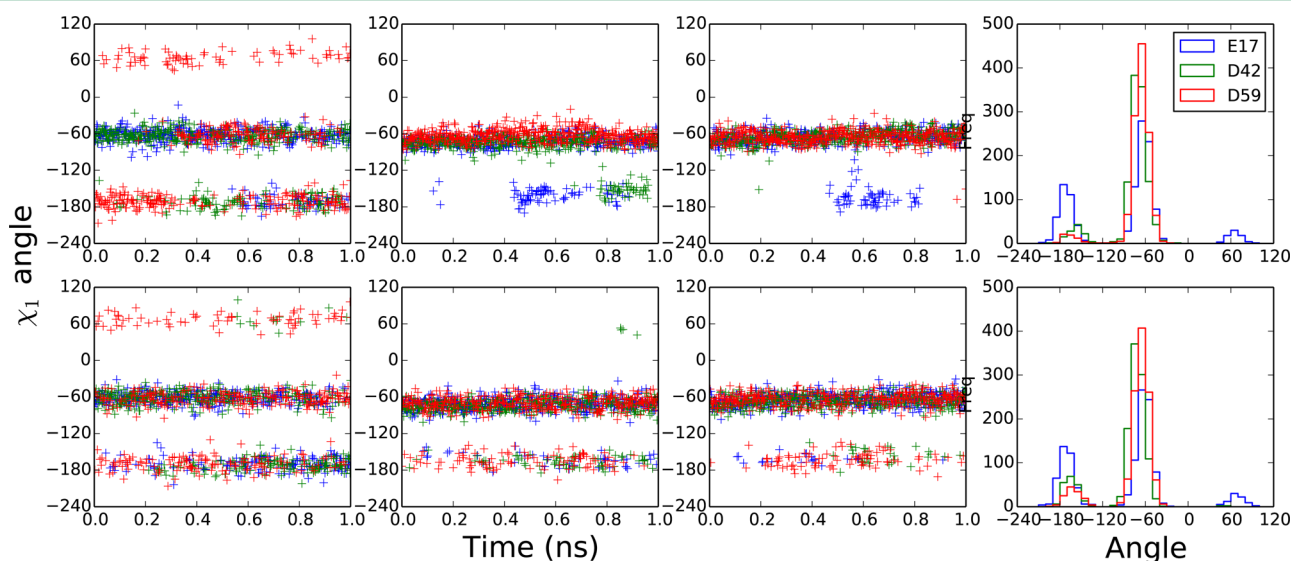


Figure 10. χ_1 angle changes of E17 (the first column), D42 (the second column), and D59 (the third column) of snake cardiotoxin obtained with the 1D (top) and 2D (bottom) EDS-HREM simulations for 1 ns at pH = 2. The fourth column represents the histograms of χ_1 angles of the three residues.

Our study shows that the 2D method enhances conformational sampling. For snake cardiotoxin, the average number of distinct and identically sized conformational clusters per pH value is 20 with the 2D EDS-HREM method and only 6 with the 1D method. When trajectories recorded at all pH values are combined, the total number of clusters is 33.3 with the 2D method and 17.7 with the 1D method. This indicates that the number of conformations sampled at all pH values increases, and this result is not simply a consequence of the redistribution of conformations sampled at individual pH values. The distribution of χ_1 angles of titratable groups shows that the 2D method allows for frequent transitions between different rotamer states, while the 1D method requires longer simulation time to observe such rotamer transitions. These results demonstrate that the 2D method can lead to a significant gain in efficiency of simulation for the same amount of total CPU time.

The new constant-pH method presented here is not a method to simultaneously estimate the pK_a of all of the sites of a large protein but instead is designed to provide accurate ensembles suitable for careful free energy studies. It is an explicit state-based approach where all relevant protonation states must be explicitly enumerated. The method is not size extensive, but the number of possible protonation states to consider is only limited by the available computational resources, with linear costs. Primary future applications are anticipated to be (1) the calculation the free energy of binding a substrate to a protein where there are protonation changes that may occur in the binding pocket or on the substrate, (2) the calculation of a quantum corrected (QM/MM) pK_a value for a key site of a complex system using a non-Boltzmann Bennett approach, (3) the computation of the free energy cost of rearranging protons as a first step in an enzymatic reaction, and (4) the accurate simulation of strongly coupled clusters of ionizable groups, such as those found in active sites, or in bioenergetic proteins.

■ ASSOCIATED CONTENT

Supporting Information

Figures showing the size distributions of the conformational clusters obtained from the trajectories of the 1D and 2D EDS-HREM simulations and schematics to explain the ART-2' clustering algorithm in detail. The Supporting Information is available free of charge on the ACS Publications website at DOI: 10.1021/ct501101f.

■ AUTHOR INFORMATION

Corresponding Author

*Phone: +1 301 5941157. E-mail: juyong.lee@nih.gov.

Funding

This research was supported by the Intramural Research Program of the National Heart, Lung, and Blood Institute, NIH.

Notes

The authors declare no competing financial interest.

■ ACKNOWLEDGMENTS

We thank Gerhard König for helpful discussions.

■ REFERENCES

- Perutz, M. F. *Science (Washington, DC, U. S.)* **1978**, *201*, 1187.
- García-Moreno, B. J. *Biol.* **2009**, *8*, 98.
- Chimentì, M. S.; Khangulov, V. S.; Robinson, A. C.; Heroux, A.; Majumdar, A.; Schlessman, J. L.; García-Moreno, B. *Structure* **2012**, *20*, 1071.
- Rastogi, V. K.; Girvin, M. E. *Nature* **1999**, *402*, 263.
- Symersky, J.; Pagadala, V.; Osowski, D.; Krah, A.; Meier, T.; Faraldo-Gómez, J. D.; Mueller, D. M. *Nat. Struct. Mol. Biol.* **2012**, *19*, 485.
- Schulz, S.; Iglesias-Cans, M.; Krah, A.; Yildiz, Ö.; Leone, V.; Matthies, D.; Cook, G. M.; Faraldo-Gómez, J. D.; Meier, T. *PLoS Biol.* **2013**, *11*, No. e1001596.
- Wang, T.; Sessions, A. O.; Lunde, C. S.; Rouhani, S.; M, R.; Duan, Y.; Facciotti, M. T. *Structure* **2013**, *21*, 290.
- Yoshikawa, S.; Muramoto, K.; Shinzawa-Itoh, K. *Annu. Rev. Biophys.* **2011**, *40*, 205.
- Tripathi, S.; Šrajer, V.; Purwar, N.; Henning, R.; Schmidt, M. *Biophys. J.* **2012**, *102*, 325.
- Isom, D. G.; Castañeda, C. A.; Cannon, B. R.; García-Moreno, B. *Proc. Natl. Acad. Sci. U. S. A.* **2011**, *108*, 5260.
- Lee, D.; Lee, J.; Seok, C. *Phys. Chem. Chem. Phys.* **2013**, *15*, 5844.
- Yang, A. S.; Gunner, M. R.; Sampogna, R.; Sharp, K.; Honig, B. *Proteins: Struct., Funct., Bioinf.* **1993**, *15*, 252.
- Alexov, E. G.; Gunner, M. R. *Biophys. J.* **1997**, *72*, 2075.
- Carstensen, T.; Farrell, D.; Huang, Y.; Baker, N. A.; Nielsen, J. E. *Proteins: Struct., Funct., Bioinf.* **2011**, *79*, 3287.
- Warwicker, J. *Proteins: Struct., Funct., Bioinf.* **2011**, *79*, 3374.
- Baptista, A. M.; Teixeira, V. H.; Soares, C. M. *J. Chem. Phys.* **2002**, *117*, 4184.
- Bürgi, R.; Kollman, P. A.; Van Gunsteren, W. F. *Proteins: Struct., Funct., Bioinf.* **2002**, *47*, 469.
- Mongan, J.; Case, D. A.; McCammon, J. A. *J. Comput. Chem.* **2004**, *25*, 2038.
- Lee, M. S.; Salsbury, F. R.; Brooks, C. L. *Proteins: Struct., Funct., Bioinf.* **2004**, *56*, 738.
- Mongan, J.; Case, D. A. *Curr. Opin. Struct. Biol.* **2005**, *15*, 157.
- Khandogin, J.; Brooks, C. L. *Biophys. J.* **2005**, *89*, 141.
- Machuqueiro, M.; Baptista, A. M. *J. Phys. Chem. B* **2006**, *110*, 2927.
- Khandogin, J.; Brooks, C. L. *Biochemistry* **2006**, *45*, 9363.
- Itoh, S. G.; Damjanović, A.; Brooks, B. R. *Proteins: Struct., Funct., Bioinf.* **2011**, *79*, 3420.
- Wallace, J. A.; Shen, J. K. *J. Chem. Theory Comput.* **2011**, *7*, 2617.
- Donnini, S.; Tegeler, F.; Groenhof, G.; Grubmüller, H. *J. Chem. Theory Comput.* **2011**, *7*, 1962.
- Goh, G. B.; Knight, J. L.; Brooks, C. L. *J. Chem. Theory Comput.* **2012**, *8*, 36.
- Sabri Dashti, D.; Meng, Y.; Roitberg, A. E. *J. Phys. Chem. B* **2012**, *116*, 8805.
- Hu, H.; Shen, L. *J. Comput. Chem.* **2014**, *35*, 1491.
- Swails, J. M.; York, D. M.; Roitberg, A. E. *J. Chem. Theory Comput.* **2014**, *10*, 1341.
- Chen, W.; Morrow, B. H.; Shi, C.; Shen, J. K. *Mol. Simul.* **2014**, *1*.
- Kong, X.; Brooks, C. L. *J. Chem. Phys.* **1996**, *105*, 2414.
- Lee, J.; Miller, B. T.; Damjanovic, A.; Brooks, B. R. *J. Chem. Theory Comput.* **2014**, *10*, 2738.
- Christ, C. D.; van Gunsteren, W. F. *J. Chem. Phys.* **2007**, *126*, No. 184110.
- Christ, C. D.; van Gunsteren, W. F. *J. Chem. Phys.* **2008**, *128*, No. 174112.
- Fukunishi, H.; Watanabe, O.; Takada, S. *J. Chem. Phys.* **2002**, *116*, 9058.
- Sugita, Y.; Kitao, A.; Okamoto, Y. *J. Chem. Phys.* **2000**, *113*, 6042.
- Mitsutake, A. *J. Chem. Phys.* **2009**, *131*, No. 094105.
- Mitsutake, A.; Okamoto, Y. *J. Chem. Phys.* **2009**, *130*, No. 214105.
- Chodera, J. D.; Shirts, M. R. *J. Chem. Phys.* **2011**, *135*, No. 194110.

- (41) Gee, J.; Shell, M. S. *J. Chem. Phys.* **2011**, *134*, No. 064112.
- (42) Jeon, J.; Shell, M. S. *Biophys. J.* **2012**, *102*, 1952.
- (43) Ostermeir, K.; Zacharias, M. *J. Comput. Chem.* **2014**, *35*, 150.
- (44) Bergonzo, C.; Henriksen, N. M.; Roe, D. R.; Swails, J. M.; Roitberg, A. E.; Cheatham, T. E., III *J. Chem. Theory Comput.* **2013**, *10*, 492.
- (45) Kokubo, H.; Tanaka, T.; Okamoto, Y. *J. Comput. Chem.* **2013**, *34*, 2601.
- (46) Chiang, C. M.; Chien, K. Y.; Lin, H. J.; Lin, J. F.; Yeh, H. C.; Ho, P. L.; Wu, W. G. *Biochemistry* **1996**, *35*, 9167.
- (47) Chiang, C. M.; Chang, S. L.; Lin, H. J.; Wu, W. G. *Biochemistry* **1996**, *35*, 9177.
- (48) Won, H.; Kim, J.; Ko, K.; Won, Y. *Bull. Korean Chem. Soc.* **2002**, *23*, 80–81.
- (49) Alexov, E.; Mehler, E. L.; Baker, N.; Baptista, A. M.; Huang, Y.; Milletti, F.; Nielsen, J. E.; Farrell, D.; Carstensen, T.; Olsson, M. H. M.; Shen, J. K.; Warwicker, J.; Williams, S.; Word, J. M. *Proteins: Struct., Funct., Bioinf.* **2011**, *79*, 3260.
- (50) Olsson, M. H. M.; Søndergaard, C. R.; Rostkowski, M.; Jensen, J. H. *J. Chem. Theory Comput.* **2011**, *7*, 525.
- (51) König, G.; Hudson, P. S.; Boresch, S.; Woodcock, H. L. *J. Chem. Theory Comput.* **2014**, *10*, 1406.
- (52) Baptista, A. M.; Martel, P. J.; Petersen, S. B. *Proteins: Struct., Funct., Bioinf.* **1997**, *27*, 523.
- (53) Baptista, A. M. *J. Chem. Phys.* **2002**, *116*, 7766.
- (54) Torrie, G.; Valleau, J. *J. Comput. Phys.* **1977**, *23*, 187.
- (55) Christ, C. D.; van Gunsteren, W. F. *J. Chem. Theory Comput.* **2009**, *5*, 276.
- (56) Nozaki, Y.; Tanford, C. *Methods Enzymol.* **1967**, *69*, 715.
- (57) Kyte, J. *Structure in Protein Chemistry*; Structure in Protein Chemistry Series; Garland: New York, NY, USA, 1995.
- (58) MacKerell, A. D.; Bashford, D.; Bellott, M.; Dunbrack, R. L.; Evanseck, J. D.; Field, M. J.; Fischer, S.; Gao, J.; Guo, H.; Ha, S.; Joseph-McCarthy, D.; Kuchnir, L.; Kuczera, K.; Lau, F. T. K.; Mattos, C.; Michnick, S.; Ngo, T.; Nguyen, D. T.; Prodhom, B.; Reiher, W. E.; Roux, B.; Schlenkrich, M.; Smith, J. C.; Stote, R.; Straub, J.; Watanabe, M.; Wirkiewicz-Kuczera, J.; Yin, D.; Karplus, M. *J. Phys. Chem. B* **1998**, *102*, 3586.
- (59) Okamoto, Y. *J. Mol. Graphics Modell.* **2004**, *22*, 425.
- (60) Kannan, S.; Zacharias, M. *Proteins: Struct., Funct., Bioinf.* **2009**, *76*, 448.
- (61) Curuksu, J.; Zacharias, M. *J. Chem. Phys.* **2009**, *130*, No. 104110.
- (62) Liu, P.; Kim, B.; Friesner, R. A.; Berne, B. J. *Proc. Natl. Acad. Sci. U. S. A.* **2005**, *102*, 13749.
- (63) Itoh, S. S. G.; Okumura, H.; Okamoto, Y. *J. Chem. Phys.* **2010**, *132*, No. 134105.
- (64) Kokubo, H.; Tanaka, T.; Okamoto, Y. *J. Comput. Chem.* **2011**, *32*, 2810.
- (65) Wallace, J. A.; Shen, J. K. *J. Chem. Phys.* **2012**, *137*, No. 184105.
- (66) Jiang, W.; Hodoscek, M.; Roux, B. *J. Chem. Theory Comput.* **2009**, *5*, 2583.
- (67) Brooks, B. R.; Brooks, C. L.; Mackerell, A. D.; Nilsson, L.; Petrella, R. J.; Roux, B.; Won, Y.; Archontis, G.; Bartels, C.; Boresch, S.; Caffisch, A.; Caves, L.; Cui, Q.; Dinner, A. R.; Feig, M.; Fischer, S.; Gao, J.; Hodoscek, M.; Im, W.; Kuczera, K.; Lazaridis, T.; Ma, J.; Ovchinnikov, V.; Paci, E.; Pastor, R. W.; Post, C. B.; Pu, J. Z.; Schaefer, M.; Tidor, B.; Venable, R. M.; Woodcock, H. L.; Wu, X.; Yang, W.; York, D. M.; Karplus, M. *J. Comput. Chem.* **2009**, *30*, 1545.
- (68) Wu, X.; Brooks, B. R. *Chem. Phys. Lett.* **2003**, *381*, 512.
- (69) Wu, X.; Hodoscek, M.; Brooks, B. R. *J. Chem. Phys.* **2012**, *137*, No. 044106.
- (70) Singhal, A. K.; Chien, K. Y.; Wu, W. G.; Rule, G. S. *Biochemistry* **1993**, *32*, 8036.
- (71) Miller, B. T.; Singh, R. P.; Klauda, J. B.; Hodoscek, M.; Brooks, B. R.; Woodcock, H. L. *J. Chem. Inf. Model.* **2008**, *48*, 1920.
- (72) Jorgensen, W. L.; Chandrasekhar, J.; Madura, J. D.; Impey, R. W.; Klein, M. L. *J. Chem. Phys.* **1983**, *79*, 926.
- (73) Chu, J.-W.; Trout, B. L.; Brooks, B. R. *J. Chem. Phys.* **2003**, *119*, 12708.
- (74) König, G.; Miller, B. T.; Boresch, S.; Wu, X.; Brooks, B. R. *J. Chem. Theory Comput.* **2012**, *8*, 3650.
- (75) Woodcock, H. L.; Miller, B. T.; Hodoscek, M.; Okur, A.; Larkin, J. D.; Ponder, J. W.; Brooks, B. R. *J. Chem. Theory Comput.* **2011**, *7*, 1208.
- (76) Nose, S. *J. Chem. Phys.* **1984**, *81*, 511.
- (77) Hoover, W. *Phys. Rev. A* **1985**, *31*, 1695.
- (78) Bogusz, S.; Cheatham, T. E.; Brooks, B. R. *J. Chem. Phys.* **1998**, *108*, 7070.
- (79) Lindstrom, M. J.; Bates, D. M. *Biometrics* **1990**, 673.
- (80) Pinheiro, J. C.; Bates, D. M. *Stat. Comput.* **1996**, *6*, 289.
- (81) Pinheiro, J.; Bates, D.; DebRoy, S.; Sarkar, D. R. *Core Team nlme: Linear and Nonlinear Mixed Effects Models*, R package version 3.1-120; R Foundation for Statistical Computing: Vienna, Austria, 2015.
- (82) R Core Team, *R: A Language and Environment for Statistical Computing*; R Foundation for Statistical Computing: Vienna, Austria, 2013.
- (83) Zuckerman, D. M.; Lyman, E. *J. Chem. Theory Comput.* **2006**, *2*, 1200.
- (84) Okur, A.; Roe, D. R.; Cui, G.; Hornak, V.; Simmerling, C. J. *J. Chem. Theory Comput.* **2007**, *3*, 557.
- (85) Roitberg, A. E.; Okur, A.; Simmerling, C. J. *Phys. Chem. B* **2007**, *111*, 2415.
- (86) Okur, A.; Miller, B. T.; Joo, K.; Lee, J.; Brooks, B. R. *J. Chem. Theory Comput.* **2013**, *9*, 1115.
- (87) Damjanović, A.; García-Moreno, B.; Lattman, E. E.; García, A. E. *Proteins: Struct., Funct., Bioinf.* **2005**, *60*, 433.
- (88) Damjanović, A.; Wu, X.; García-Moreno, B.; Brooks, B. R. *Biophys. J.* **2008**, *95*, 4091.
- (89) Damjanović, A.; Brooks, B. R.; García-Moreno, B. J. *Phys. Chem. A* **2011**, *115*, 4042.
- (90) Karpen, M. E.; Tobias, D. J.; Brooks, C. L. *Biochemistry* **1993**, *32*, 412.
- (91) Carpenter, G. A.; Grossberg, S. *Appl. Opt.* **1987**, *26*, 4919.
- (92) Pao, Y.-H. *Adaptive Pattern Recognition and Neural Networks*; Addison-Wesley Longman: Boston, MA, USA, 1989.